AIMS Mathematics, 11(7): 21819–21845.
DOI:10.3934/math.2026883
Received: 18 March 2026
Revised: 01 July 2026
Accepted: 07 July 2026
Published: 22 July 2026

https://www.aimspress.com/journal/Math

Research article

Oral drug kinetics under first-pass metabolism: A fractional modeling framework

Shadiya Nasrin K. B.[1], **J. Kokila**[1,*] **and M. Z. Youssef**[2,*]

[1] Department of Statistics and Applied Mathematics, Central University of Tamil Nadu, Thiruvarur 610005, India

[2] Department of Mathematics and Statistics, College of Science, Imam Mohammad Ibn Saud Islamic University (IMSIU), P.O. Box 65892, Riyadh 11566, Saudi Arabia

* **Correspondence:** Email: kokimaths@gmail.com, mzabouelyamin@imamu.edu.sa.

Abstract: This study proposes compartment models with the Caputo fractional derivative to capture drug dynamics across absorption, central, and peripheral compartments, and to account for memory effects and anomalous kinetics. The first part of the study covers mathematical modeling, which enables analysis of the amount of drug in each compartment using closed-form expressions. The second part is to estimate the pharmacokinetic parameters and compare models using the Akaike information criterion and Bayesian information criterion for the drugs pindolol, fenoprofen, and cyclosporin A. The regression analysis was performed by using the corresponding Mittag-Leffler regression model and the trust-region algorithm with the Adams predictor-corrector method.

Keywords: pharmacokinetics; absorption; mathematical modeling; Mittag-Leffler function; Laplace transform; inverse problems; nonlinear least squares method
Mathematics Subject Classification: 33E12, 44A10, 60J70, 65L09, 92C45, 93A30, 93E24

1. Introduction

Extravascular drug administration encompasses delivery routes where absorption into systemic circulation requires traveling at least one biological membrane. Among these, oral administration is the most prevalent, accommodating drugs in solid, liquid, or other dosage forms. Upon ingestion, orally administered drugs encounter the gastrointestinal (GI) tract, composed of the buccal cavity, esophagus, stomach, small intestine, and large intestine. The GI membrane serves as a critical absorption interface, exhibiting spatial heterogeneity in pH, enzymatic activity, electrolyte composition, surface properties, and fluid viscosity. These variations, coupled with structural adaptations such as villi and microvilli in the small intestine, dramatically increase absorptive surface

area and account for the small intestine's dominant role in systemic uptake [1].

For absorption to occur, the drug must be in solution; thus, dissolution of tablets begins in the stomach, where residence time ranges from 0.5 to 2 hours before gastric emptying into the duodenum. Although the stomach supports limited absorption, favorable only for certain lipophilic or weakly acidic drugs, most absorption occurs in the duodenum, jejunum, and proximal ileum. Gastric emptying is accelerated under fasting conditions but delayed postprandially, impacting drug transfer kinetics. The intestinal epithelial barrier, comprising lipids, proteins, lipoproteins, and polysaccharides, selectively allows molecular passage while restricting others [1].

Two primary mechanisms govern GI absorption: passive diffusion and active transport. Passive diffusion, the dominant pathway for most drugs, drives molecular transfer along the concentration gradient from luminal fluids into systemic circulation, adhering to first-order kinetics. Conversely, active transport employs carrier proteins to translocate drug molecules, often against concentration gradients, before release into the bloodstream. Due to finite carrier availability, active transport demonstrates saturation kinetics: first-order behavior at low solute concentrations, transitioning to zero-order at higher concentrations. At low solute concentration, absorption follows first-order kinetics, and at high solute concentration, absorption follows zero-order kinetics [1]. These mechanistic distinctions, alongside GI physiological variability, collectively dictate the rate, extent, and consistency of drug absorption.

Patient-to-patient variability in drug absorption arises from the interplay between a substance's physicochemical characteristics and host-specific physiological conditions. Zhou [2] examined the factors affecting the absorption, categorizing the mechanisms in which drugs traverse biological barriers, while Abuhelwa et al. [3] detailed how gastrointestinal (GI) pH gradients and food intake modulate oral drug absorption. Their work also compared empirical absorption models with more advanced "mechanism-based" frameworks that integrate physiological parameters. Complementary studies [4, 5] highlighted the complex interactions within the GI environment that shape the absorption kinetics of orally administered drugs. Key determinants include the gastric emptying rate, intestinal transit time, segmental pH variations, and distribution of membrane transporters and metabolic enzymes [6].

Following absorption into the hepatic portal system, drugs may undergo first-pass hepatic metabolism before reaching systemic circulation. This biotransformation can substantially diminish bioavailability, particularly for drugs with high hepatic extraction ratios [7]. Notably, even compounds with high intestinal permeability and efficient absorption can exhibit low systemic exposure if they are subject to extensive first-pass metabolism [8]. Thus, the ultimate oral bioavailability reflects a combined effect of the absorption process and presystemic metabolism. The work in [9] investigated how physicochemical properties, such as solubility, lipophilicity, and molecular size-shape, affect oral bioavailability profiles across different drug classes.

In parallel, mathematical modeling approaches have evolved to capture different types of complex processes [10–16]. Early pharmacokinetic models are often empirical, relying on statistical fits to plasma concentration-time data [17, 18], but more recent efforts incorporate biological accuracy. For instance, the GI-Sim model [19] represents a mechanistic, physiology-based platform for simulating drug absorption across distinct GI segments. These advanced models integrate factors such as luminal dissolution, intestinal transit, pH-dependent solubility, and transporter-mediated uptake. The applications of advanced mathematical analysis and fractional calculus in studying complex systems

are widely reported in the literature [20–23]. The literature reflects a clear progression toward physiologically based pharmacokinetic (PBPK) and absorption modeling; several studies [24–26] addressed only narrow aspects of absorption. Motivated by the literature, the present absorption study extends the modeling approach based on [23, 27].

In [28], Wenlock estimated pharmacokinetic parameters for 215 drugs, and in [29], introduced absorption modeling, which includes advanced formulation techniques to overcome the limitations in oral drug delivery and enhance the therapeutic effect. To the best of our knowledge, the fractional kinetics of absorption modeling are not documented in the literature. Motivated by this fact and the work in [29], this novel study explores the application of fractional kinetics in absorption modeling and drug analysis for corresponding models. The contributions from this study are the following:

- This novel study analyzes the drug concentration level in each compartment using the exact solution representation derived by the Laplace transform method.
- This study investigates the fractional-order compartment modeling for the real drugs pindolol [30], fenoprofen calcium [31], and cyclosporin A [32], respectively.
- The memory effect and anomalous kinetics for the amount of drug-time profiles of the drugs are successfully studied and compared by using Mittag-Leffler regression models and the trust-region algorithm with the Adams predictor-corrector method.
- This novel study enables us to investigate the first-pass metabolism, absorption, and elimination rate constants for the data in an effective way.
- The fractional model approach improves the model flexibility and the Mittag-Leffler function model ensures the best data fit, which optimizes the drug dosing strategies and understanding of the individual variabilities.

2. Preliminaries

This section provides the mathematical foundation in fractional calculus necessary for the development of the main results.

Definition 2.1. *[33–35] Let f be an absolutely continuous function defined on the interval $[a, b]$. For $0 < \alpha < 1$, $f \mapsto \frac{d^\alpha f}{dt^\alpha}$ denotes the Caputo fractional derivative and it is defined as*

$$\frac{d^\alpha f}{dt^\alpha} := \frac{1}{\Gamma(1-\alpha)} \int_a^t (t-s)^{-\alpha} f'(s) ds, \ t \in (a, b], \tag{2.1}$$

where $f' = \frac{df}{dt}$.

Definition 2.2. *[33–35] Let $\lambda \in \mathbb{R}, t \in [a, b]$, where $a, b \geq 0$, $\alpha > 0$, and $\beta > 0$. The ML function $E_{\alpha,\beta}(-\lambda t^\alpha)$ is defined by*

$$E_{\alpha,\beta}(-\lambda t^\alpha) := \sum_{k=0}^{\infty} \frac{(-\lambda t^\alpha)^k}{\Gamma(\alpha k + \beta)}. \tag{2.2}$$

If $\beta = 1$, the above expression (2.2) changes to

$$E_\alpha(-\lambda t^\alpha) := \sum_{k=0}^{\infty} \frac{(-\lambda t^\alpha)^k}{\Gamma(\alpha k + 1)}. \tag{2.3}$$

To facilitate the derivation of the analytical solutions, we first present the Laplace transform of ML functions (2.2) and (2.3) and their properties, which are central to the current fractional modeling framework.

Theorem 2.1. *[33–35] For $\alpha > 0$, $\beta > 0$, $\lambda \in \mathbb{R}$, let the two-parameter Mittag-Leffler function be as in* (2.2)*. Then the Laplace transform of the Mittag-Leffler function is given by*

(i) $\mathcal{L}\{E_\alpha(\pm\lambda t^\alpha)\}(s) = \frac{s^{\alpha-1}}{s^\alpha \mp \lambda}, Re(s) > |\lambda|^{\frac{1}{\alpha}}$,
(ii) $\mathcal{L}\left\{t^{\alpha-1}E_{\alpha,\alpha}(\pm\lambda t^\alpha)\right\}(s) = \frac{1}{s^\alpha \mp \lambda}, Re(s) > |\lambda|^{\frac{1}{\alpha}}$.

Theorem 2.2. *[33–35] For $\alpha > 0$, $\beta > 0$, $\lambda \in \mathbb{R}$, let the two-parameter Mittag-Leffler function be as in* (2.2)*. Then the ML function satisfies the following results:*

i. $t \mapsto E_{\alpha,\beta}(-\lambda t^\alpha) \in L^1[a, b]$ *and hence*

$$\int_0^t \tau^{\alpha-1}E_{\alpha,\alpha}(-\lambda\tau^\alpha)d\tau = \frac{1}{\lambda}[1 - E_\alpha(-\lambda t^\alpha)].$$

ii. $\int_0^t \tau^{\gamma-1}E_{\alpha,\gamma}(-y\tau^\alpha)(t-\tau)^{\beta-1}E_{\alpha,\beta}(-z(t-\tau)^\alpha)d\tau = \frac{t^{\beta+\gamma-1}}{y-z}\left[yE_{\alpha,\gamma+\beta}(-yt^\alpha) - zE_{\alpha,\gamma+\beta}(-zt^\alpha)\right]$.
iii. $\lambda t^\alpha(E_{\alpha,\alpha+1}(\lambda t^\alpha)) = E_{\alpha,1}(\lambda t^\alpha) - 1$.

2.1. Analysis and solution methods for fractional differential equations

For $0 < \alpha < 1$ and $c > 0$, let the fractional differential equation be of the following form:

$$\frac{d^\alpha x}{dt^\alpha} = -c, t > 0, \tag{2.4}$$

where c is a constant. The following theorem gives the solution for $x(t)$ using the Laplace transform technique.

Theorem 2.3. *For $0 < \alpha < 1$ and $c > 0$, let the fractional differential equation be of the form of (2.4) with initial data $x(0) = X_0$. Then the solution of the equation is given by*

$$x(t) = X_0 - \frac{ct^\alpha}{\Gamma(\alpha+1)}. \tag{2.5}$$

Proof. Applying the Laplace transform on (2.4), we get

$$\mathcal{L}\{x(t)\}(s) = \frac{X_0}{s} - \frac{c}{s^{\alpha+1}}. \tag{2.6}$$

Inverting the transform gives

$$x(t) = X_0 - \frac{ct^\alpha}{\Gamma(\alpha+1)}. \tag{2.7}$$

□

For $0 < \alpha < 1$ and $a > 0$, let another form of the fractional differential equation be as follows:

$$\frac{d^\alpha x}{dt^\alpha} = -ax(t) + f(t), t > 0. \tag{2.8}$$

Theorem 2.4. *For $0 < \alpha < 1$ and $a > 0$, let the fractional differential equation be of the form of (2.8) with initial data $x(0) = X_0$. Then the solution of the equation is given by*

$$x(t) = X_0 E_\alpha(-at^\alpha) + \int_0^t f(t-\tau)\tau^{\alpha-1}E_{\alpha,\alpha}(-a\tau^\alpha)d\tau. \tag{2.9}$$

Proof. Applying the Laplace transform on (2.8), we get

$$X(s) = \frac{s^{\alpha-1}}{s^\alpha + a}X_0 + \frac{F(s)}{s^\alpha + a}, \tag{2.10}$$

where

$$F(s) = \mathcal{L}\{f(t)\}.$$

Inverting the transform and implementing results (i) and (ii) of Theorem (2.1), we get

$$x(t) = X_0 E_\alpha(-at^\alpha) + \int_0^t f(t-\tau)\tau^{\alpha-1}E_{\alpha,\alpha}(-a\tau^\alpha)d\tau. \tag{2.11}$$

□

For $0 < \alpha < 1$, $a > 0$, and $b > 0$, let the system of fractional differential equations be as follows:

$$\frac{d^\alpha x}{dt^\alpha} = -ax(t), t > 0, \tag{2.12}$$

$$\frac{d^\alpha y}{dt^\alpha} = ax(t) - by(t), t > 0. \tag{2.13}$$

Theorem 2.5. *For $0 < \alpha < 1$, $a > 0$, and $b > 0$, let the fractional differential equation be of the form of (2.12) and (2.13) with initial data $x(0) = X_0$, $y(0) = 0$. Then the solution of the system is given by*

$$x(t) = X_0 E_\alpha(-at^\alpha), \tag{2.14}$$

$$y(t) = \frac{X_0 a}{(b-a)}(E_\alpha(-at^\alpha) - E_\alpha(-bt^\alpha)). \tag{2.15}$$

Proof. By using the results of Theorem 2.4, we get

$$x(t) = X_0 E_\alpha(-at^\alpha), \tag{2.16}$$

$$y(t) = a\int_0^t x(\tau)(t-\tau)^{\alpha-1}E_{\alpha,\alpha}(-b(t-\tau)^\alpha)d\tau. \tag{2.17}$$

Considering the value of $x(t)$ from (2.16), we have

$$y(t) = X_0 a\int_0^t E_{\alpha,1}(-a\tau^\alpha)(t-\tau)^{\alpha-1}E_{\alpha,\alpha}(-b(t-\tau)^\alpha)d\tau. \tag{2.18}$$

Further, results (ii) and (iii) of Theorem (2.2) reduce the above expression to

$$y(t) = \frac{X_0 a}{(b-a)}(E_\alpha(-at^\alpha) - E_\alpha(-bt^\alpha)). \tag{2.19}$$

Hence the proof is complete. □

3. Absorption models

In pharmacokinetics, we can conceptually divide the human body into different compartments to picturize the movement of drugs. Each compartment represents a group of tissues or organs, and it provides a better understanding and prediction of the drug's parameters, which is valuable in clinical practice [1].

3.1. Two-compartment model

We consider two-compartment pharmacokinetic models, which contain the absorption compartment (small intestine) and the central compartment (blood). The administered drug is absorbed from the small intestine (A) to the central compartment (B) at a rate of k_a and eliminated from B at a rate of k_e with the assumption of $k_a > k_e$. Figure 1 represents the schematic diagram for the two-compartment absorption model.

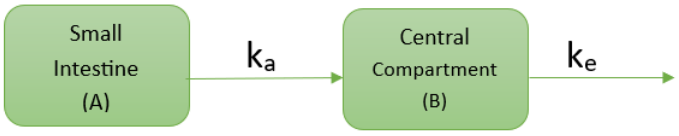

Figure 1. Schematic diagram for the two-compartment model.

The absorption takes place as either a zero-order or a first-order process.

Remark 1. *Throughout the study, we consider the case where $k_a > k_e$, which represents the standard absorption-elimination process. The case where $k_a < k_e$ corresponds to the exceptional phenomenon known as flip-flop kinetics, and when $k_a = k_e$, the model requires a different parameter-estimation procedure [1]. Therefore, these special cases are excluded from the subsequent analysis.*

3.1.1. Zero-order model

For $0 < \alpha < 1$, the rate of change of the amount of drug in the two-compartment, zero-order absorption model (that is, the compartment A is saturated) can be represented as

$$\frac{d^\alpha A}{dt^\alpha} = -z, \tag{3.1}$$

$$\frac{d^\alpha B}{dt^\alpha} = zF_h - k_e B(t), \tag{3.2}$$

where z is the saturated absorption rate and F_h is the fraction escaping first-pass metabolism [29]. The following theorem establishes the solution representation for the above system for some $t \in [0, T]$.

Theorem 3.1. *For $0 < \alpha < 1$, $z > 0$, $F_h > 0$, $k_e > 0$, and $t \in [0, T]$, let the linear system of fractional differential equations be of the form of (3.1) and (3.2) with initial data $A(0) = A_0$, $B(0) = 0$. Then the solution of the system is given by*

$$A(t) = A_0 - \frac{zt^\alpha}{\Gamma(\alpha + 1)}, \tag{3.3}$$

$$B(t) = \frac{zF_h}{k_e}(1 - E_\alpha(-k_e t^\alpha)). \tag{3.4}$$

Remark 2. *It should be mentioned here that the positivity of A(t) holds for* $A_0\Gamma(\alpha+1) - zt^\alpha > 0$. *Thus, there exists* $t^* > 0$ *of the form* $t^* = \left(\frac{A_0\Gamma(\alpha+1)}{z}\right)^{1/\alpha}$ *such that A(t) takes the expression as*

$$A(t) = \begin{cases} A_0 - \frac{zt^\alpha}{\Gamma(\alpha+1)} & , \quad t < t^*, \\ 0 & , \quad t \geq t^*. \end{cases}$$

3.1.2. First-order model

If compartment A is unsaturated, then first-order absorption takes place, and the system will become

$$\frac{d^\alpha A}{dt^\alpha} = -k_a A(t), \tag{3.5}$$

$$\frac{d^\alpha B}{dt^\alpha} = F_h k_a A(t) - k_e B(t). \tag{3.6}$$

The following theorem characterizes the solution of the above system by providing its representation for $t \in [0, T]$.

Theorem 3.2. *Let* k_a *and* k_e *be such that* $k_a > k_e > 0$ *and for* $0 < \alpha < 1$, $F_h > 0$, *and* $t \in [0, T]$, *the linear system of fractional differential equations be of the form of (3.5) and (3.6) with initial data* $A(0) = A_0$, $B(0) = 0$. *Then the solution of the system is given by*

$$A(t) = A_0 E_\alpha(-k_a t^\alpha), \tag{3.7}$$

$$B(t) = \frac{A_0 F_h k_a}{(k_e - k_a)}(E_\alpha(-k_a t^\alpha) - E_\alpha(-k_e t^\alpha)). \tag{3.8}$$

The proofs of Theorems 3.1 and 3.2 are essentially identical to that of the previous Theorems 2.3–2.5 and are therefore omitted.

3.2. Three-compartment model

We consider three-compartment models, which divide the body into three compartments: the absorption compartment (small intestine), the central compartment (blood), and the peripheral compartment (tissues/organs). The movement of the drug from the small intestine to the central compartment is irreversible, and movement between the central compartment and the peripheral compartment is reversible. Figure 2 represents the schematic diagram for the three-compartment absorption model.

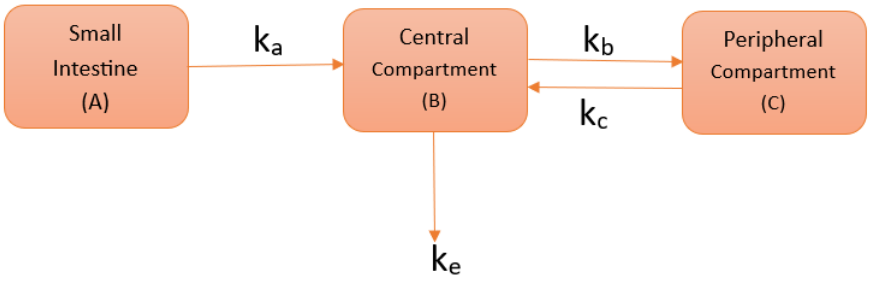

Figure 2. Schematic diagram for the three-compartment model.

3.2.1. Zero-order model

For $0 < \alpha < 1$, the rate of change of the amount of drug in the three-compartment zero-order absorption model with $A(0) = A_0$ and $B(0) = C(0) = 0$ can be represented as

$$\frac{d^\alpha A}{dt^\alpha} = -z, \tag{3.9}$$

$$\frac{d^\alpha B}{dt^\alpha} = zF_h - k_b B(t) + k_c C(t) - k_e B(t), \tag{3.10}$$

$$\frac{d^\alpha C}{dt^\alpha} = k_b B(t) - k_c C(t). \tag{3.11}$$

The following theorem proves the solution representation for the above system for $t \in [0, T]$.

Theorem 3.3. *For $0 < \alpha < 1$, $z > 0$, $F_h > 0$, $k_b > 0$, $k_c > 0$, $k_e > 0$, and $t \in [0, T]$, let the linear system of fractional differential equations be of the form of (3.9)–(3.11) with initial data $A(0) = A_0$ and $B(0) = C(0) = 0$. Then the solution of the system is given by*

$$A(t) = A_0 - \frac{zt^\alpha}{\Gamma(\alpha+1)}, \tag{3.12}$$

$$B(t) = zF_h\Big(\frac{k_c}{\lambda_1\lambda_2} - \frac{E_\alpha(-\lambda_1 t^\alpha)(k_c-\lambda_1)}{\lambda_1(\lambda_2-\lambda_1)} + \frac{E_\alpha(-\lambda_2 t^\alpha)(k_c-\lambda_2)}{\lambda_2(\lambda_2-\lambda_1)}\Big), \tag{3.13}$$

$$C(t) = zF_h k_b\Big(\frac{1}{\lambda_1\lambda_2} - \frac{E_\alpha(-\lambda_1 t^\alpha)}{\lambda_1(\lambda_2-\lambda_1)} + \frac{E_\alpha(-\lambda_2 t^\alpha)}{\lambda_2(\lambda_2-\lambda_1)}\Big), \tag{3.14}$$

where

$$\lambda_1 = \frac{1}{2}[(k_b + k_c + k_e) + \sqrt{(k_b + k_c + k_e)^2 - 4k_c k_e}], \tag{3.15}$$

$$\lambda_2 = \frac{1}{2}[(k_b + k_c + k_e) - \sqrt{(k_b + k_c + k_e)^2 - 4k_c k_e}]. \tag{3.16}$$

Proof. Applying the Laplace transform on (3.9), we get

$$\mathcal{L}\{A(t)\}(s) = \frac{A_0}{s} - \frac{z}{s^{\alpha+1}}. \tag{3.17}$$

Inverting the transform gives

$$A(t) = A_0 - \frac{zt^\alpha}{\Gamma(\alpha+1)}. \tag{3.18}$$

Similarly, application of the Laplace transform on (3.10) and (3.11) along with the initial data $B(0) = C(0) = 0$ yields

$$\mathcal{L}\{B(t)\}(s) = \frac{zF_h}{s(s^\alpha + k_b + k_e)} + \frac{k_c C(s)}{(s^\alpha + k_b + k_e)}, \tag{3.19}$$

$$\mathcal{L}\{C(t)\}(s) = \frac{k_b B(s)}{s^\alpha + k_c}. \tag{3.20}$$

With simplification of (3.19) and (3.20), we get

$$\mathcal{L}\{B(t)\}(s) = \frac{zF_h(s^\alpha + k_c)}{[(s^\alpha + \lambda_1)(s^\alpha + \lambda_2)]s}, \tag{3.21}$$

$$\mathcal{L}\{C(t)\}(s) = \frac{zF_h k_b}{[(s^\alpha + \lambda_1)(s^\alpha + \lambda_2)]s}, \tag{3.22}$$

where λ_1 and λ_2 are given by (3.15) and (3.16). Further, using the Laplace transform of the convolution of functions and result (i) of Theorem (2.2), we get the required result:

$$B(t) = zF_h\Big(\frac{k_c}{\lambda_1\lambda_2} - \frac{E_\alpha(-\lambda_1 t^\alpha)(k_c - \lambda_1)}{\lambda_1(\lambda_2 - \lambda_1)} + \frac{E_\alpha(-\lambda_2 t^\alpha)(k_c - \lambda_2)}{\lambda_2(\lambda_2 - \lambda_1)}\Big), \tag{3.23}$$

$$C(t) = zF_h k_b\Big(\frac{1}{\lambda_1\lambda_2} - \frac{E_\alpha(-\lambda_1 t^\alpha)}{\lambda_1(\lambda_2 - \lambda_1)} + \frac{E_\alpha(-\lambda_2 t^\alpha)}{\lambda_2(\lambda_2 - \lambda_1)}\Big). \tag{3.24}$$

Hence the proof is complete. □

3.2.2. First-order model

If compartment A is unsaturated, then absorption will turn into a first-order process, and the system for the process will be taken as

$$\frac{d^\alpha A}{dt^\alpha} = -k_a A(t), \tag{3.25}$$

$$\frac{d^\alpha B}{dt^\alpha} = F_h k_a A(t) - k_b B(t) + k_c C(t) - k_e B(t), \tag{3.26}$$

$$\frac{d^\alpha C}{dt^\alpha} = k_b B(t) - k_c C(t). \tag{3.27}$$

The following theorem provides a representation of the solution to the above system for $t \in [0, T]$.

Theorem 3.4. *For $0 < \alpha < 1$, $F_h > 0$, $k_a > 0$, $k_b > 0$, $k_c > 0$, $k_e > 0$, and $t \in [0, T]$, let the linear system of fractional differential equations be of the form of (3.25)–(3.27) with initial data $A(0) = A_0$ and $B(0) = C(0) = 0$. Then the solution of the system is given by*

$$A(t) = A_0 E_\alpha(-k_a t^\alpha), \tag{3.28}$$

$$B(t) = A_0 F_h k_a\Big(\frac{(k_c - \lambda_1)E_\alpha(-\lambda_1 t^\alpha)}{(\lambda_2 - \lambda_1)(k_a - \lambda_1)} + \frac{(k_c - \lambda_2)E_\alpha(-\lambda_2 t^\alpha)}{(\lambda_1 - \lambda_2)(k_a - \lambda_2)} + \frac{(k_c - k_a)E_\alpha(-k_a t^\alpha)}{(\lambda_1 - k_a)(\lambda_2 - k_a)}\Big), \tag{3.29}$$

$$C(t) = \frac{A_0 F_h k_a k_b}{(\lambda_2 - \lambda_1)(k_a - \lambda_1)(k_a - \lambda_2)}\Big((k_a - \lambda_2)E_\alpha(-\lambda_1 t^\alpha) - (k_a - \lambda_1)E_\alpha(-\lambda_2 t^\alpha) - (\lambda_1 - \lambda_2)\,E_\alpha(-k_a t^\alpha)\Big). \tag{3.30}$$

Proof. The proof of this theorem is similar to that of the previous theorem. Hence, it is omitted. □

The proposed method can potentially be extended to handle incommensurate versions of the proposed models, where different state variables have distinct fractional orders ($\alpha \neq \beta \neq \gamma$) [36, 37].

4. Numerical analysis of drug absorption

Understanding a drug's ADME (Absorption, Distribution, Metabolism, and Excretion) characteristics is fundamental for predicting therapeutic efficacy and optimizing dosage regimens. In pharmacokinetics, compartmental modeling provides a quantitative framework for simulating the drug's movement through various physiological spaces and is particularly useful for evaluating absorption behavior.

In this study, drug absorption is analyzed using two- and three-compartment models, with explicit analytical solutions provided in the previous section. The resulting time-course profiles in Figures 3 and 4 illustrate the sequential transfer of the drug from the absorption site into systemic circulation, followed by elimination.

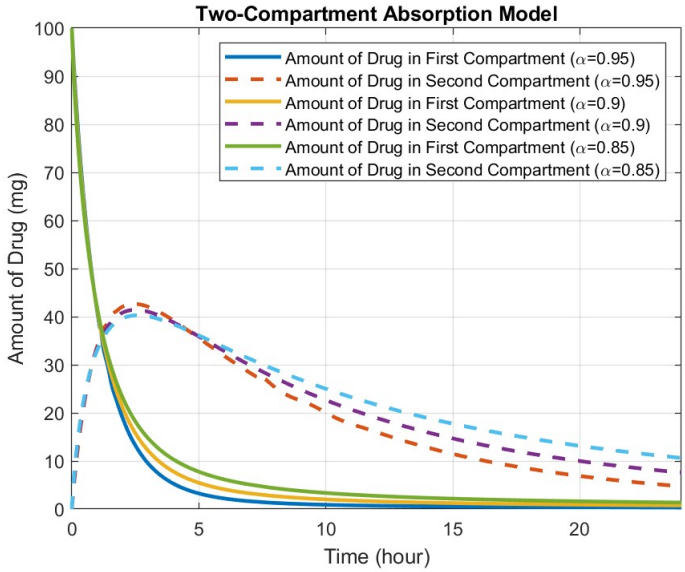

Figure 3. Drug pattern for the two-compartment model for different values of α with fixed $A_0 = 100$ mg, $F_h = 0.628$, $k_a = 0.898$, and $k_e = 0.148$ over the time period [0,24].

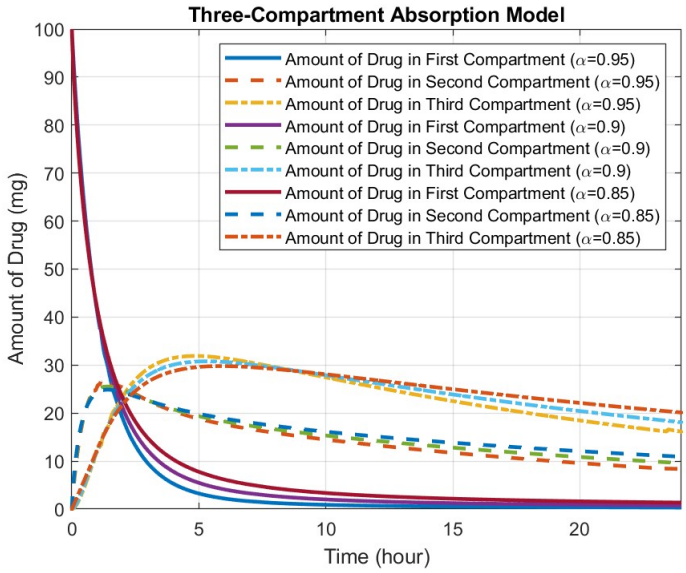

Figure 4. Drug pattern for the three-compartment model for different values of α with fixed $A_0 = 100$ mg, $F_h = 0.68$, $k_a = 0.898$, $k_b = 0.788$, $k_c = 0.451$, $k_e = 0.148$, $\lambda_1 = 1.3371$, and $\lambda_2 = 0.0499$ over the time period [0,24].

In the two-compartment model (Figure 3), the absorption compartment (small intestine) initially loaded with the administered 100-mg dose, shows a rapid decline, approaching zero within approximately 10–15 hours. Notably, the quantity falls below 10 mg before 5 hours post-administration, indicating efficient absorption and distribution. The central compartment exhibits a delayed rise, peaking within 5 hours, followed by gradual elimination. At 24 hours, drug levels remained around 7 mg for $\alpha = 0.9$, reflecting sustained systemic presence due to slower elimination kinetics. For $\alpha = 0.95$, the drug decline curve from the central compartment is steeper than the other two.

The first-order, three-compartment model reveals a more nuanced pharmacokinetic profile, which can be seen in Figure 4. As in the two-compartment case, the absorption compartment declines steeply, while the central compartment follows a similar but slightly attenuated peak profile. The additional peripheral compartment exhibits a faster accumulation phase, reaching approximately 30 mg at 5 hours, and maintains detectable drug levels for a prolonged period. This extended terminal phase reflects distribution into and gradual release from peripheral tissues. A decrease in α values increases the rate at which the amount declines in the peripheral compartments, suggesting faster elimination of the drug.

Overall, the two-compartment model effectively captures primary absorption and systemic distribution, whereas the three-compartment model provides a more physiologically realistic depiction, incorporating faster tissue equilibration and extended drug residence time. This added complexity is critical for accurately predicting pharmacokinetic parameters, optimizing dosage intervals, and minimizing the risk of subtherapeutic exposure or toxicity in clinical applications.

5. Parameter estimation for drug data

This section presents the parameter estimation for the orally administered drugs, pindolol, fenoprofen calcium, and cyclosporin A using a first-order absorption process in two- and three-compartment models with the fractional derivative.

5.1. Pindolol

Pindolol is a non-selective β-adrenergic blocker (β-blocker) widely used for hypertension and certain cardiovascular disorders. It is rapidly absorbed from the gastrointestinal tract and undergoes first-pass metabolism, yet it exhibits a longer duration of action than many other β-adrenoceptor blockers such as propranolol and alprenolol. This extended duration enables once-daily dosing in hypertension management [38]. The pharmacological mechanisms of pindolol, including its cardiac and skeletal muscle effects, have been discussed in detail in [39]. Gugler et al. [30] conducted a clinical pharmacokinetic (PK) study, estimating PK parameters for both oral and intravenous (IV) administration with the help of pindolol concentration data with respect to time.

The amount of pindolol is calculated by using the following relation between the concentration pattern and the amount of drug for the concentration profiles, which is available in [30].

$$C = \frac{FD}{V}, \tag{5.1}$$

where C is the concentration at time t, F is the bioavailability, D is the administered dose, and V is the volume of distribution. The data fitting has been performed in two ways:

- Method 1: A nonlinear regression model in the view of the Mittag-Leffler function, which is given by
$$B_{ijk} = \frac{A_0 F_h k_a}{(k_e - k_a)}(E_\alpha(-k_a t_k^\alpha) - E_\alpha(-k_e t_k^\alpha)) + \epsilon_{ijk}, \tag{5.2}$$
where B_{ijk} is the observation taken at time t_k for the i^{th} subject in time period j.

- Method 2: The trust-region algorithm with the Adams predictor-corrector (PC) method.

The parameter estimation procedure for a PK compartment model using the Adams PC method [34] is summarized in Algorithm 1.

Algorithm 1 Adams PC algorithm for parameter estimation

1: Fix initial guess on rate constants of the concerned model together with fractional order α (which are to be estimated).
2: Set initial concentrations as per the available data.
3: Solve the fractional system using the Adams PC method and interpolate the solution at the observed time points.
4: Fit the model to the data using $lsqcurvefit$ and extract the fitted parameters.
5: Calculate the AIC and BIC for model prediction.
6: Plot the real data along with the regression line.
7: Display the fitted parameters, AIC, and BIC.

The estimated parameter values and model comparison matrices for pindolol, obtained using both approaches, are compared to assess the robustness of the model. Figures 5–14 viasualize the pindolol data-fitting for the ten subjects. Table 1 lists the estimated parameters: fraction escaping first-pass metabolism (F_h), absorption rate constant (k_a), elimination rate constant (k_e), and fractional order α. Most of the subjects exhibit F_h values close to 1.0 (range: 0.6863–1.2051) from both methods, indicating nearly complete systemic availability post-first-pass metabolism. The absorption rate constant (k_a) from the Mittag-Leffler regression model varies substantially (0.8071–5.8001), with Subject 4 showing the fastest absorption. For the ML regression model, elimination rate constant (k_e) ranges from 0.1253 to 0.300, where a lower k_e (e.g., Subject 1) reflects prolonged systemic presence, while a higher k_e (e.g., Subject 10) indicates rapid clearance. Fractional orders α from both methods (0.883-0.999) capture non-integer kinetics and drug memory effects. The confidence intervals (CIs) offer additional insight into the statistical uncertainty of the parameter estimates. The 95% confidence intervals for the estimated parameters of Subject 1 are given in Table 2.

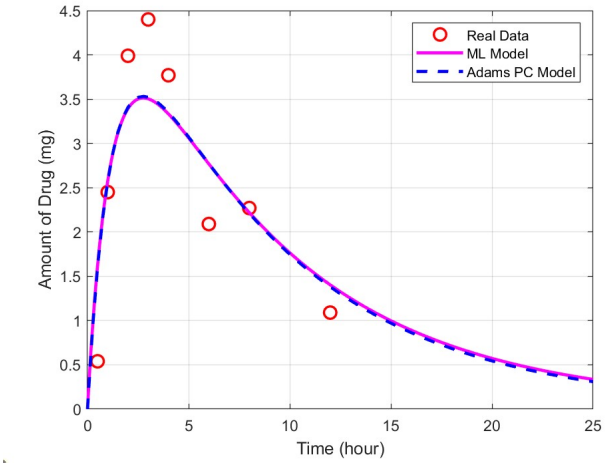

Figure 5. Fitted pindolol model for patient 1.

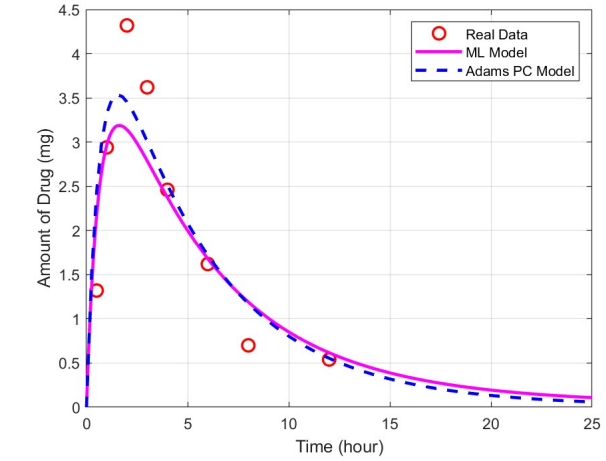

Figure 6. Fitted pindolol model for patient 2.

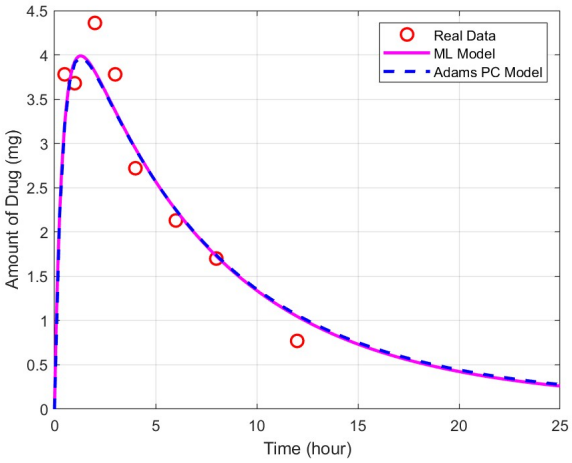

Figure 7. Fitted pindolol model for patient 3.

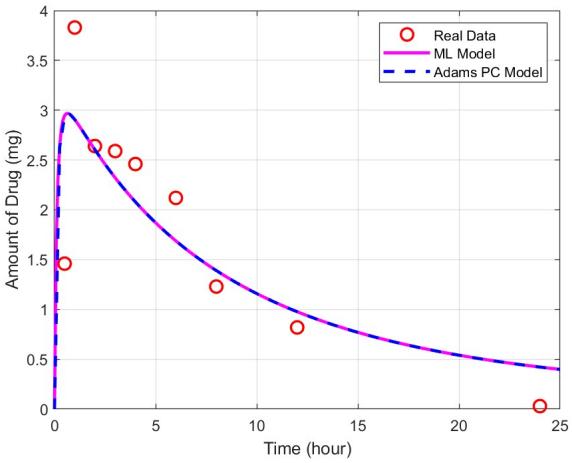

Figure 8. Fitted pindolol model for patient 4.

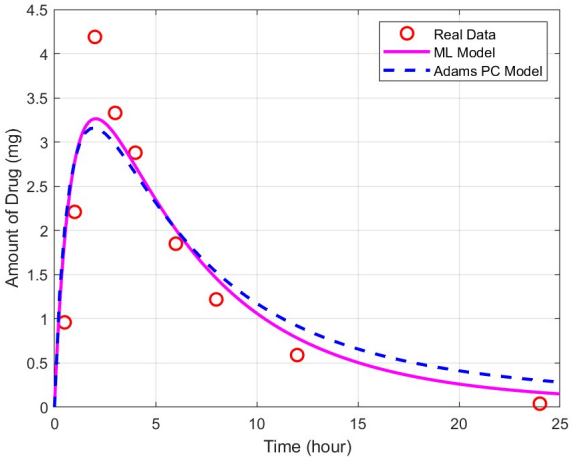

Figure 9. Fitted pindolol model for patient 5.

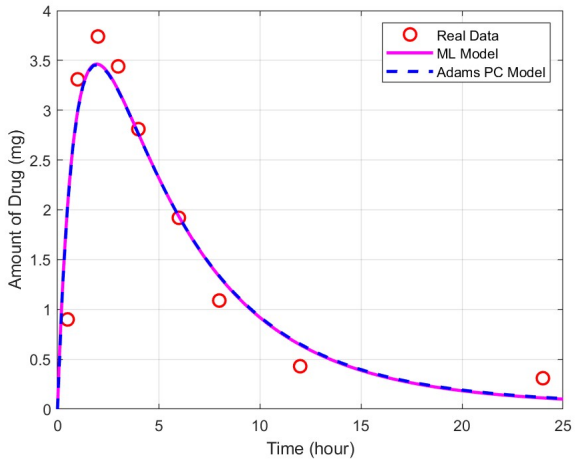

Figure 10. Fitted pindolol model for patient 6.

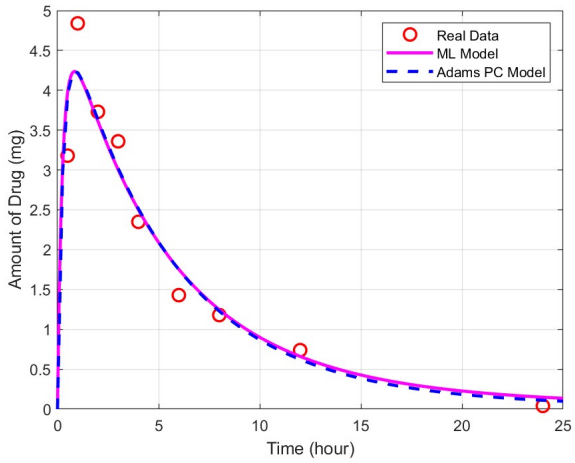

Figure 11. Fitted pindolol model for patient 7.

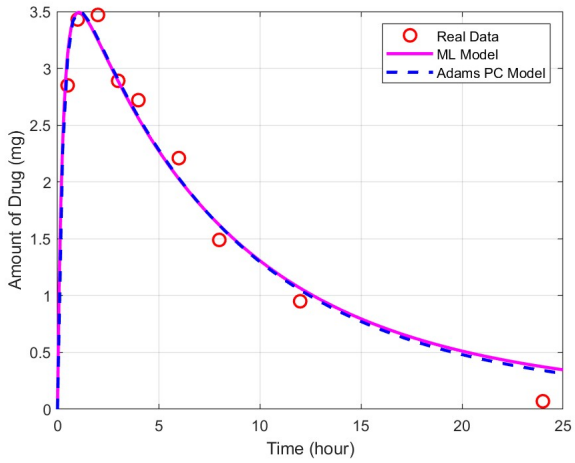

Figure 12. Fitted pindolol model for patient 8.

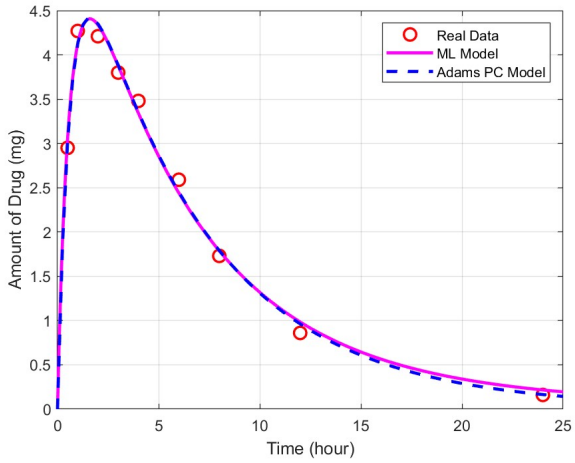

Figure 13. Fitted pindolol model for patient 9.

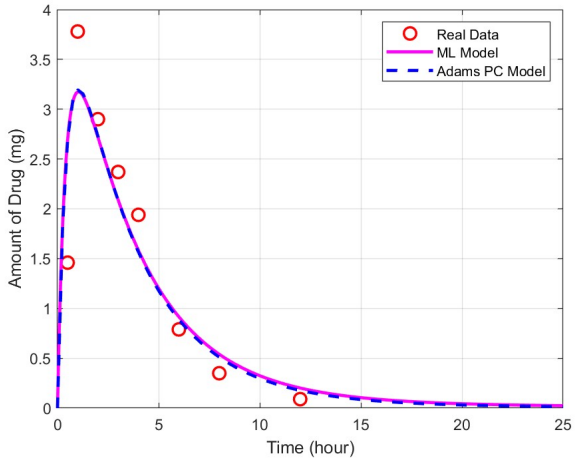

Figure 14. Fitted pindolol model for patient 10.

Table 1. Estimated parameter values and model prediction of pindolol after oral administration of 5 mg for 10 subjects.

Subject		F_h	k_a	k_e	α	AIC	BIC
1	Method 1	1.000	0.8071	0.1253	0.983	-1.58	-1.34
	Method 2	1.000	0.8042	0.1244	0.990	0.17	0.49
2	Method 1	0.9000	1.4001	0.2000	0.967	-1.69	-1.45
	Method 2	0.9705	1.5000	0.2000	0.990	-0.58	-0.27
3	Method 1	1.000	2.2001	0.1562	0.956	-10.58	-10.34
	Method 2	1.000	2.2000	0.1576	0.950	-8.34	-8.02
4	Method 1	0.6863	5.8001	0.1500	0.883	-2.07	-1.48
	Method 2	0.6866	5.800	0.1500	0.883	-0.09	0.70
5	Method 1	0.9944	1.001	0.1959	0.961	-6.37	-5.78
	Method 2	1.0379	1.0000	0.2248	0.900	-1.91	-1.12
6	Method 1	1.0845	1.001	0.2211	0.969	-9.08	-8.49
	Method 2	1.0873	1.0000	0.2227	0.966	-6.96	-6.17
7	Method 1	1.037	3.5001	0.2083	0.955	-11.29	-10.69
	Method 2	1.0219	3.5000	0.1975	0.975	-9.86	-9.07
8	Method 1	0.8462	3.001	0.1477	0.927	-24.38	-23.79
	Method 2	0.8357	3.0000	0.1400	0.945	-23.85	-23.06
9	Method 1	1.2051	1.5001	0.1821	0.964	-33.07	-32.47
	Method 2	1.1562	1.5771	0.1637	0.999	-32.28	-31.49
10	Method 1	0.8812	2.2001	0.300	0.971	-4.35	-4.11
	Method 2	0.8823	2.2000	0.3000	0.987	-2.44	-2.13

Table 2. Estimated 95% confidence intervals for pindolol (Subject 1).

Parameter	95% CI
F_h	(0.59726–1.3653)
k_a	(0.35693–1.4431)
k_e	(0.073954–0.15991)
α	(0.90233–1.0631)

The small difference between the estimated parameter values and their confidence-interval limits indicates that the estimates are well-constrained by the data. The model performance is assessed by the Akaike information criterion (AIC) and the Bayesian information criterion (BIC) [40]. For a fitted model, AIC and BIC values can be calculated by using the following expressions:

$$AIC = n * log\Big(\frac{resnorm}{n}\Big) + 2 * k, \tag{5.3}$$

$$BIC = n * log\Big(\frac{resnorm}{n}\Big) + log(n) * k. \tag{5.4}$$

Here, n is the number of datapoints, k is the number of fitted parameters, and $resnorm$ is the residual sum of squares obtained from nonlinear least squares estimation. Negative AIC and BIC values for all

subjects from the ML regression model analysis confirm good model fit, with Subject 9 yielding the lowest values and Subject 1 the highest (less negative). For all the subjects, method 1 possesses lower AIC and BIC values than the other.

5.2. *Fenoprofen calcium*

Fenoprofen, marketed as Nalfon, is a nonsteroidal anti-inflammatory drug (NSAID) indicated for rheumatoid arthritis, osteoarthritis, and general pain relief. A one-compartment open model effectively describes its oral PK profile [41]. Based on Eq (5.1), the post-dose amounts of orally administered fenoprofen calcium [31] are calculated. Similar to the drug pindolol, the parameter estimation for fenoprofen has been done in two ways, and the parameter values are compared and tabulated (Table 3).

Table 3. Estimated parameter values and model prediction of fenoprofen after oral administration of 60 mg, 165 mg, and 300 mg.

Dose		F_h	k_a	k_e	α	AIC	BIC
60 mg	Method 1	0.7000	3.4001	0.2800	0.969	44.75	46.45
	Method 2	0.7039	3.0001	0.2800	0.95	44.97	47.23
165 mg	Method 1	0.7496	2.4001	0.3113	0.948	69.80	71.49
	Method 2	0.8087	2.0001	0.3500	0.900	72.78	75.04
300 mg	Method 1	0.7000	2.5001	0.2700	0.925	87.19	88.88
	Method 2	0.7001	2.0000	0.2800	0.880	87.64	89.90

Data fitting with the ML regression model (5.2) gives an excellent fit across all doses compared with the second method (Figures 15–17). The absorption rate constant (k_a) ranges from 2.40 to 3.40 from method 1, with the 60-mg dose showing the fastest absorption, and 2.0001 to 3.0001 from method 2. Elimination rate constants (k_e) are relatively consistent (0.2700–0.3500), while α values (0.900–0.969) suggest the uniform fractional kinetics across doses from both methods. The fraction escaping first-pass metabolism (F_h) is highest for the 165-mg dose (0.7496), estimated from method 2. The estimated confidence intervals of the parameters obtained for 60 mg are summarized in Table 4.

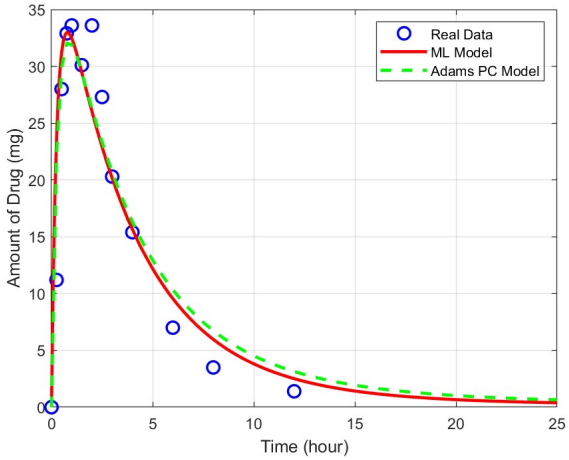

Figure 15. Fitted fenoprofen model for a dose of 60 mg.

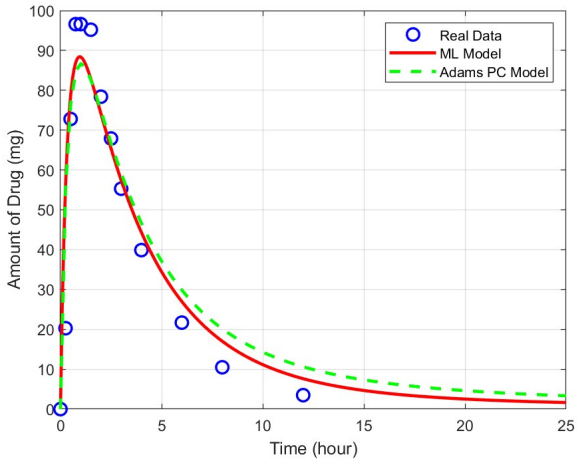

Figure 16. Fitted fenoprofen model for a dose of 165 mg.

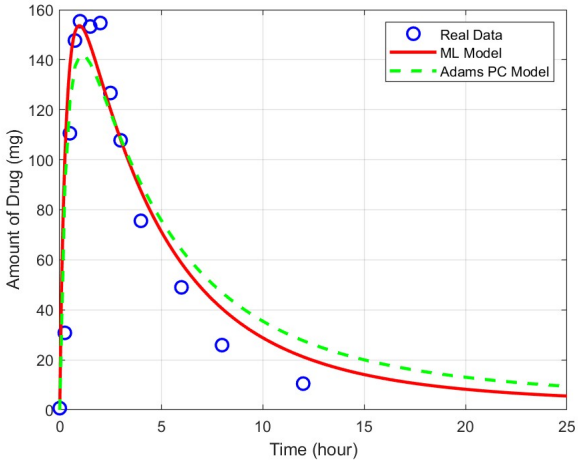

Figure 17. Fitted fenoprofen model for a dose of 300 mg.

Table 4. Estimated 95% confidence intervals for fenoprofen at 60 mg.

Parameter	95% CI
F_h	(0.59438–0.85187)
k_a	(2.0952–3.9048)
k_e	(0.22398–0.33602)
α	(0.88789–1.0493)

The confidence intervals are relatively narrow, demonstrating that the estimated parameter values exhibit limited variability. For each dose of fenoprofen, lower AIC and BIC values are produced by the ML regression model than the other one. Although AIC and BIC values increased with the dose, indicating greater residual variability at higher doses, the overall low values from method 1 confirm excellent model fit. These results emphasize dose-dependent absorption kinetics and measurable

deviations from classical PK models.

5.3. *Cyclosporin A*

Cyclosporin A (CsA) is a lipophilic immunosuppressant essential in preventing organ transplant rejection (kidney, liver, heart, etc.). Its PK properties, such as bioavailability (F), clearance (CL), and volume of distribution (V), are highly variable and influenced by food, bile, and concomitant drugs [42]. CsA distribution depends on both physicochemical traits and biological carriers. As reported in [43], CsA exhibits unusual aqueous solubility inversely correlated with temperature, a key limitation for oral dosing. The amount of cyclosporin A after a single 300-mg oral dose is calculated using data from [32] and by the relation (5.1). The Mittag-Leffler regression model (for the three-compartment model) for data-fitting is

$$\begin{aligned} B_{ijk} &= A_0 F_h k_a \Big(\frac{(k_c-\lambda_1)E_\alpha(-\lambda_1 t_k^\alpha)}{(\lambda_2-\lambda_1)(k_a-\lambda_1)} + \frac{(k_c-\lambda_2)E_\alpha(-\lambda_2 t_k^\alpha)}{(\lambda_1-\lambda_2)(k_a-\lambda_2)} \\ &\quad + \frac{(k_c-k_a)E_\alpha(-k_a t_k^\alpha)}{(\lambda_1-k_a)(\lambda_2-k_a)} \Big) + \epsilon_{ijk}, \end{aligned} \tag{5.5}$$

where B_{ijk} is the observation taken at time t_k for the i^{th} subject in time period j.

The three-compartment Mittag-Leffler regression model (5.5) (method 1) and the trust-region algorithm with the Adams PC method (method 2) are employed for the data-fitting and comparison of parameters (Figures 18–23). Cyclosporin has a poor absorption rate, exhibiting incomplete absorption in the intestine. Table 5 summarizes the estimated PK parameter values, along with the fractional order α and model performance indexes, AIC and BIC, from two methods. Across all the subjects, the regression line shows strong agreement with experimental data during the absorption and elimination phases. For example, Subject A gets its peak at 5 hours, while Subjects D and E exhibit rapid peaks with steeper declines from both methods. Moderate peaks are observed in Subjects B, C, and F, where the models still track observed data despite scatter.

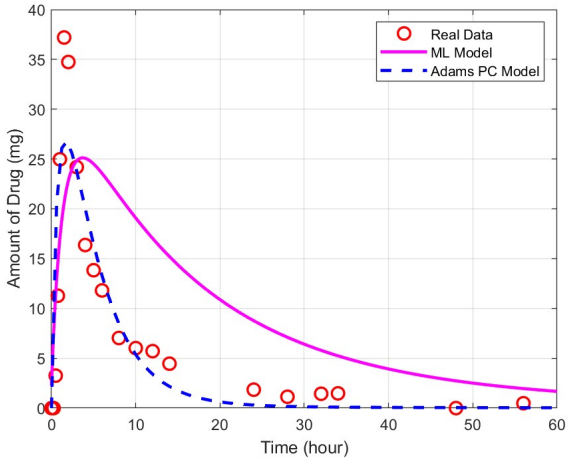

Figure 18. Fitted cyclosporin model for patient A.

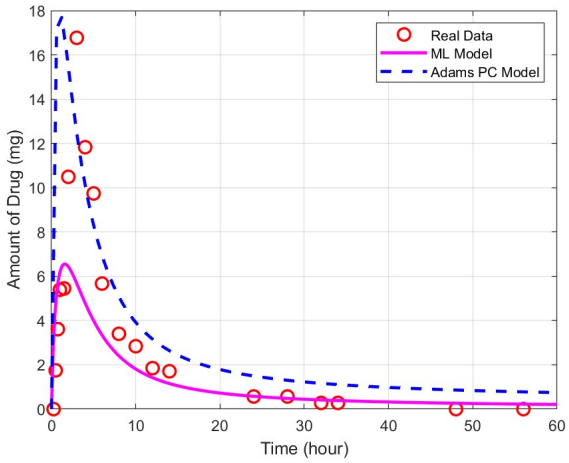

Figure 19. Fitted cyclosporin model for patient B.

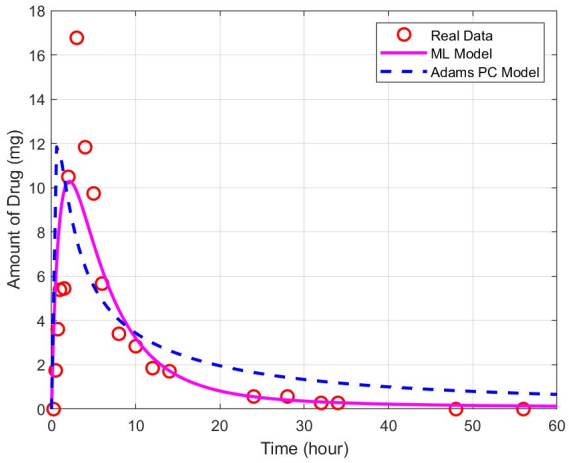

Figure 20. Fitted cyclosporin model for patient C.

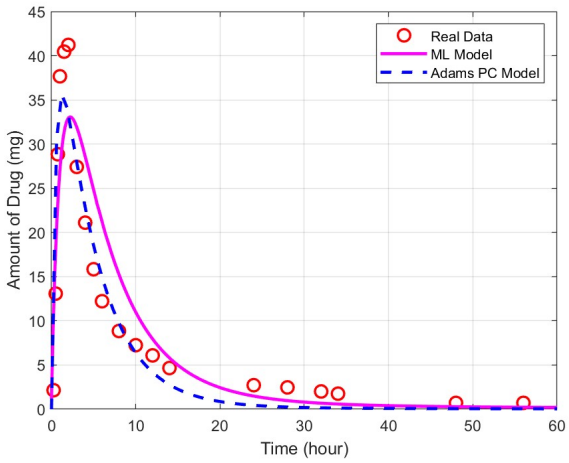

Figure 21. Fitted cyclosporin model for patient D.

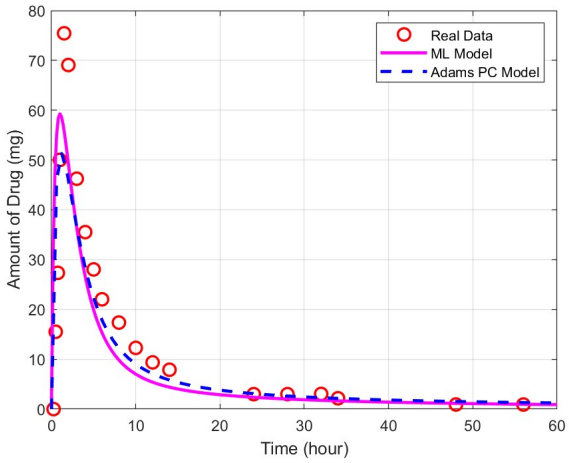

Figure 22. Fitted cyclosporin model for patient E.

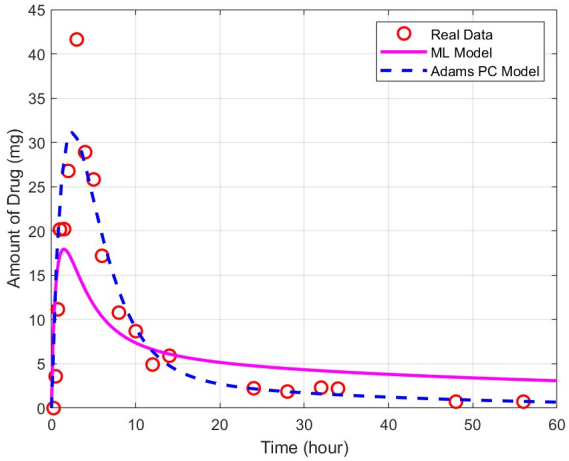

Figure 23. Fitted cyclosporin model for patient F.

Table 5. Estimated parameter values and model prediction of cyclosporin A after oral administration of 300 mg for 8 subjects.

Sub.		F_h	k_a	k_b	k_c	k_e	α	AIC	BIC
A	Method 1	0.2800	0.7001	0.0067	0.7926	0.0707	0.954	102.16	107.39
	Method 2	0.2800	0.7000	0.8537	1.9999	0.4753	0.99	86.11	92.38
B	Method 1	0.7000	0.4581	0.0338	0.1050	0.7762	0.85	60.95	65.93
	Method 2	0.5000	0.3900	1.000	0.0100	1.000	0.85	88.56	94.53
C	Method 1	0.2000	0.8001	$0.368 * 10^{-9}$	0.1000	0.2493	0.937	48.72	53.70
	Method 2	0.2000	0.8000	1.000	0.3000	1.000	0.80	74.84	80.81
D	Method 1	0.4000	0.8581	0.0006	0.8991	0.1963	0.970	81.25	86.23
	Method 2	0.4000	0.8000	0.9632	0.9000	0.5532	0.99	81.28	87.26
E	Method 1	0.4000	1.5001	0.0309	0.0500	0.5060	0.9	119.74	124.72
	Method 2	0.5198	0.8000	0.0000005	1.000	0.8000	0.838	115.60	121.58
F	Method 1	1.000	0.5111	0.7078	0.0900	0.222	0.854	96.75	101.73
	Method 2	0.4000	0.3000	0.1820	0.0500	0.3857	0.989	76.29	82.27

Estimated parameters show the marked inter-subject variability. F_h values range from 0.2000 to 1.000 for the Mittag-Leffler regression model and from 0.2000 to 0.5198 for the second method. The highest absorption rate (k_a) and lowest distribution rate (k_c) occur in Subject E from the ML regression model analysis (1.5001 and 0.0500, respectively). Fractional order α varied widely, reflecting heterogeneous deviation from classical kinetics. Subject D has the highest α from both methods. For the estimated parameters F_h, k_a, k_b, k_c, k_e, and α, the confidence intervals (for Subject A) are consolidated in Table 6.

Table 6. Estimated 95% confidence intervals for cyclosporin A (Subject A).

Parameter	95% CI
F_h	(-3.2668–3.9268)
k_a	(0.0085246–1.3915)
k_b	(-6.9115–6.9149)
k_c	(-325.3–326.89)
k_e	(-0.7801–0.9805)
α	(0.85323–1.0557)

The parameters contain a wide range of 95% confidence intervals. AIC and BIC values confirmed model adequacy, with Subject E possessing the highest, likely due to data scatter. Out of six subjects, three exhibit the lowest AIC and BIC values from method 1, while the remaining three show the lowest values from the alternative method. These findings underscore the importance of fractional modeling in capturing CsA's highly variable, clinically critical PK behavior.

6. Conclusions

The present study demonstrates the inclusion of fractional order α into pharmacokinetic modeling and the accurate prediction of ADME profiles for orally administered drugs, especially first-pass metabolism. The successful application of analytical solutions for both the zero- and first-order absorption models, incorporating fractional derivatives, enables precise characterization of drug dynamics. The exact solution enhances interpretability and enables parameter estimation, thereby increasing the robustness of PK analysis. Parameter estimation has been done for the drugs pindolol, fenoprofen, and cyclosporin A, which have distinct physicochemical properties and PK characteristics, using the Mittag-Leffler regression model and Adams PC algorithm. For pindolol, a drug with high oral bioavailability and rapid absorption, data-fitting captures the early rises in the amount of drug, followed by extended elimination from both methods. The pharmacokinetic evaluation of fenoprofen calcium capsules demonstrates rapid absorption and prolongs the existence of the drug in the central compartment as well. For both pindolol and fenoprofen, the ML model gives the best fit for all the subjects compared to the other method. In the case of cyclosporin A, the results obtained from both methods vary for most of the subjects. The estimated F_h values provide quantitative insights into the degree of first-pass metabolism, considering the inter-subject variability in drug exposure. For all datasets, the parameter α allows for capturing the memory effects and anomalous kinetics, leading to improved goodness of fit. The reduced AIC and BIC values from method 1 support the model improvement over method 2 in most of the subjects. In summary, the fractional-order absorption models effectively captured the key pharmacokinetic aspects, including rate constants, rapid absorption, and prolonged elimination. The smoothness and authenticity of the model curves emphasize the importance of fractional calculus in PK modeling.

Author contributions

Shadiya Nasrin K B: Methodology, resources, formal analysis, investigation, software, writing—original draft, writing—review and editing; J. Kokila: Conceptualization, formal analysis, validation, supervision, writing—review and editing; Maged Z. Youssef: Writing—review and editing.

Use of Generative-AI tools declaration

The authors declare that they have not used Artificial Intelligence (AI) tools in the creation of this article.

Conflict of interest

All authors declare no conflicts of interest in this paper.

References

1. S. S. Jambhekar, P. J. Breen, *Basic pharmacokinetics*, London: Pharmaceutical Press, 2009.
2. H. Zhou, Pharmacokinetic strategies in deciphering atypical drug absorption profiles, *J. Clin. Pharmacol.*, **43** (2003), 211–227. https://doi.org/10.1177/0091270002250613

3. A. Y. Abuhelwa, D. B. Williams, R. N. Upton, D. J. Foster, Food, gastrointestinal pH, and models of oral drug absorption, *Eur. J. Pharm. Biopharm*, **112** (2017), 234–248. https://doi.org/10.1016/j.ejpb.2016.11.034
4. L. Cheng, H. Wong, Food effects on oral drug absorption: Application of physiologically-based pharmacokinetic modeling as a predictive tool, *Pharmaceutics*, **12** (2020), 672. https://doi.org/10.3390/pharmaceutics12070672
5. D. Fleisher, C. Li, Y. Zhou, L. H. Pao, A. Karim, Drug, meal and formulation interactions influencing drug absorption after oral administration: clinical implications, *Clin. Pharmacokinet.*, **36** (1999), 233–254. https://doi.org/10.2165/00003088-199936030-00004
6. G. Lamberti, S. Cascone, F. Marra, G. Titomanlio, M. d'Amore, A. A. Barba, Gastrointestinal behavior and ADME phenomena: II. In silico simulation, *J. Drug Deliv. Sci. Tec.*, **35** (2016), 165–171. https://doi.org/10.1016/j.jddst.2016.06.014
7. Y. K. Tam, Individual variation in first-pass metabolism, *Clin. Pharmacokinet.*, **25** (1993), 300–328. https://doi.org/10.2165/00003088-199325040-00005
8. D. J. Back, S. M. Rogers, First-pass metabolism by the gastrointestinal mucosa, *AP&T*, **1** (1987), 339–357. https://doi.org/10.1111/j.1365-2036.1987.tb00634.x
9. M. V. Varma, R. S. Obach, C. Rotter, H. R. Miller, G. Chang, S. J. Steyn, et al., Physicochemical space for optimum oral bioavailability: contribution of human intestinal absorption and first-pass elimination, *J. Med. Chem.*, **53** (2010), 1098–1108. https://doi.org/10.1021/jm901371v
10. J. Kokila, M. Vellappandi, D. Meghana, V. Govindaraj, Optimal control study on Michaelis-Menten kinetics-A fractional version, *Math. Comput. Simul.*, **210** (2023), 571–592. https://doi.org/10.1016/j.matcom.2023.03.033
11. X. Wu, W. Zhang, X. S. Wang, J. Li, A mechanistic model-to-model approach for solving a nonlinear pharmacokinetic model, *Bull. Malays. Math. Sci. Soc.*, **48** (2025), 53. https://doi.org/10.1007/s40840-025-01827-3
12. B. Shiri, Well-posedness of the mild solutions for incommensurate systems of delay fractional differential equations, *Fractal Fract.*, **9** (2025), 60. https://doi.org/10.3390/fractalfract9020060
13. M. A. Zaky, A new endpoint-adaptive spectral method for nonlinear tempered fractional terminal value problems with non-smooth solutions, *Appl. Numer. Math.*, **225** (2026), 76–86. https://doi.org/10.1016/j.apnum.2026.02.003
14. M. A. Zaky, A linearized two-dimensional Galerkin-L1 spectral method with diagonalization for time-fractional diffusion equations with delay, *Appl. Numer. Math.*, **220** (2026), 1–12. https://doi.org/10.1016/j.apnum.2025.09.008
15. S. Kumawat, S. Bhatter, B. Bhatia, S. D. Purohit, H. M. Baskonus, D. L. Suthar, Novel application of q-HAGTM to analyze Hilfer fractional differential equations in diabetic dynamics, *Math. Comput. Simul.*, **238** (2025), 136–149. https://doi.org/10.1016/j.matcom.2025.04.029
16. S. Kumawat, S. Bhatter, S. D. Purohit, D. L. Suthar, Mathematical modeling of tuberculosis using Caputo fractional derivative: A comparative analysis with real data, *Sci. Rep.*, **15** (2025), 12672. https://doi.org/10.1038/s41598-025-97502-5

17. A. D'Ambrosio, F. Itaj, F. Cacace, V. Piemonte, Mathematical modeling of the gastrointestinal system for preliminary drug absorption assessment, *Bioengineering*, **11** (2024), 813. https://doi.org/10.3390/bioengineering11080813

18. M. Pompa, M. Capocelli, V. Piemonte, A new gastro-intestinal mathematical model to study drug bioavailability, *Med. Eng. Phys.*, **74** (2019), 106–114. https://doi.org/10.1016/j.medengphy.2019.09.015

19. E. Sjögren, J. Westergren, I. Grant, G. Hanisch, L. Lindfors, H. Lennernäs, et al., In silico predictions of gastrointestinal drug absorption in pharmaceutical product development: Application of the mechanistic absorption model GI-Sim, *Eur. J. Pharm. Sci.*, **49** (2013), 679–698. https://doi.org/10.1016/j.ejps.2013.05.019

20. S. J. Achar, T. Sathiyaraj, S. Harshavarthini, Fractional order modelling of water scarcity and its social effects, *Model. Earth Syst. Environ.*, **11** (2025), 335. https://doi.org/10.1007/s40808-025-02510-z

21. M. Jan, K. T. Kubra, S. H. Farooqi, A. Asghar, A mathematical approach to multi-route drug distribution via compartmental models, *Model. Earth Syst. Environ.*, **11** (2025), 385. https://doi.org/10.1007/s40808-025-02571-0

22. V. Singh, P. Thakur, S. K. Srivastava, A nonlinear time-fractional-order epidemic model for tobacco smoking with sensitivity analysis, *Model. Earth Syst. Environ.*, **11** (2025), 318. https://doi.org/10.1007/s40808-025-02468-y

23. M. Vellappandi, S. Lee, Role of fractional derivatives in pharmacokinetic/pharmacodynamic anesthesia model using BIS data, *Comput. Biol. Med.*, **187** (2025), 109783. https://doi.org/10.1016/j.compbiomed.2025.109783

24. S. Bhatter, K. Jangid, S. D. Purohit, Fractionalized mathematical models for drug diffusion, *Chaos Soliton. Fract.*, **165** (2022), 112810. https://doi.org/10.1016/j.chaos.2022.112810

25. A. Dokoumetzidis, R. Magin, P. Macheras, Fractional kinetics in multi-compartmental systems, *J. Pharmacokinet. Pharmacodyn*, **37** (2010), 507–524. https://doi.org/10.1007/s10928-010-9170-4

26. V. F. Morales-Delgado, M. A. Taneco-Hernández, C. Vargas-De-León, J. F. Gómez-Aguilar, Exact solutions to fractional pharmacokinetic models using multivariate Mittag-Leffler functions, *Chaos Soliton. Fract.*, **168** (2023), 113164. https://doi.org/10.1016/j.chaos.2023.113164

27. D. Verotta, Fractional compartmental models and multi-term Mittag–Leffler response functions, *J. Pharmacokinet. Pharmacodyn.*, **37** (2010), 209–215. https://doi.org/10.1007/s10928-010-9155-3

28. M. C. Wenlock, Profiling the estimated plasma concentrations of 215 marketed oral drugs, *Med. Chem. Commun.*, **7** (2016), 706–719. https://doi.org/10.1039/C5MD00583C

29. M. C. Wenlock, Oral drug suitability parameters, *Med. Chem. Commun.*, **9** (2018), 460–470. https://doi.org/10.1039/C7MD00586E

30. R. Gugler, W. Herold, H. J. Dengler, Pharmacokinetics of pindolol in man, *Eur. J. Clin. Pharmacol.*, **7** (1974), 17–24. https://doi.org/10.1007/bf00614385

31. J. F. Nash, L. D. Bechtol, R. J. Bopp, K. Z. Farid, C. T. Spradlin, C. A. Bunde, Linear pharmacokinetics of orally administered fenoprofen calcium, *J. Pharm. Sci.*, **68** (1979), 1087–1090. https://doi.org/10.1002/jps.2600680907

32. J. Grevel, E. Nüesch, E. Abisch, K. Kutz, Pharmacokinetics of oral cyclosporin A (Sandimmun) in healthy subjects, *Eur J. Clin. Pharmacol.*, **31** (1986), 211–216. https://doi.org/10.1007/bf00606661

33. L. Debnath, D. Bhatta, *Integral transforms and their applications*, New York: Chapman and Hall/CRC, 2016. https://doi.org/10.1201/9781420010916

34. K. Diethelm, *The analysis of fractional differential equations: An application oriented exposition using differential operators of Caputo type*, Berlin: Springer, 2010. https://doi.org/10.1007/978-3-642-14574-2

35. I. Podlubny, *Fractional differential equations: an introduction to fractional derivatives, fractional differential equations, to methods of their solution and some of their applications*, Elsevier, 1998.

36. B. Shiri, Y. G. Shi, D. Baleanu, The well-posedness of incommensurate FDEs in the space of continuous functions, *Symmetry*, **16** (2024), 105. https://doi.org/10.3390/sym16081058

37. D. Baleanu, J. J. Nieto, B. Shiri, Gronwall inequality for incommensurate systems of weakly singular integral equations and its application to FDEs, *Differ. Integral Equ.*, **39** (2026), 1–14. https://doi.org/10.57262/die039-0102-1

38. W. H. Aellig, Clinical pharmacology of pindolol, *Am. Heart J.*, **104** (1982), 346–356. https://doi.org/10.1016/0002-8703(82)90125-9

39. B. J. Clark, K. Menninger, A. Bertholet, Pindolol-the pharmacology of a partial agonist, *Brit. J. Clin. Pharmaco.*, **13** (1982), 149S–158S. https://doi.org/10.1111/j.1365-2125.1982.tb01904.x

40. D. C. Montgomery, E. A. Peck, G. G. Vining, *Introduction to linear regression analysis*, John Wiley & Sons, 2021.

41. C. K. Ward, R. E. Schirmer, Fenoprofen calcium, *Anal. Profiles Drug Substances*, **6** (1977), 161–182. https://doi.org/10.1016/S0099-5428(08)60344-5

42. A. Fahr, Cyclosporin clinical pharmacokinetics, *Clin. Pharmacokinet.*, **24** (1993), 472–495. https://doi.org/10.2165/00003088-199324060-00004

43. G. Ismailos, C. Reppas, J. B. Dressman, P. Macheras, Unusual solubility behaviour of cyclosporin A in aqueous media, *J. Pharm. Pharmacol.*, **43** (1991), 287–289. https://doi.org/10.1111/j.2042-7158.1991.tb06688.x

AIMS Press